ACS APPLIED MATERIALS & INTERFACES

www.acsami.org

Research Article

Anisotropic Triboelectric Nanogenerator Based on Ordered Electrospinning

Ning Wang,[⊥] Xiao-Xiong Wang,[⊥] Kang Yan, Weizhi Song, Zhiyong Fan, Miao Yu, and Yun-Ze Long*

Cite This: *ACS Appl. Mater. Interfaces* 2020, 12, 46205−46211

Read Online

ACCESS | Metrics & More | Article Recommendations | Supporting Information

ABSTRACT: As a new type of energy harvesting and conversion device, nanogenerator can collect various energies from daily life environment and convert it into electrical energy; it has great flexibility and can provide power for small independent systems. The triboelectric nanogenerator (TENG) is widely concerned because of their high output energy density. However, in the case of an open circuit, there will be static charge accumulation on the friction surface. The high voltage generated by the accumulation of charge on the surface will bring the risk of electrostatic discharge (ESD) to nearby circuits. To solve this problem, we have used the ordered polymer nanofibers obtained by electrospinning technology to form an anisotropic triboelectric nanogenerator with better tensile properties and mechanical strength than disordered electrospinning TENG. By adjusting the effective contact area, the voltage output in the longitudinal direction is one order of magnitude higher than the voltage output in the lateral direction. When not in use, the nanogenerator can be rotated 90°, so static charge accumulation and circuit burnout can be avoided, providing an easy method of preventing ESD in a wearable environment.

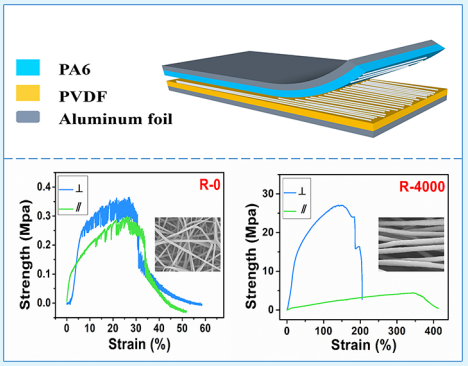

KEYWORDS: *triboelectric nanogenerator, anisotropy, electrostatic discharge, electrospinning, fiber membrane*

1. INTRODUCTION

With the rapid increase in the number of portable electronic devices, the research and development of energy sources attracts increasing interests.[1−4] Electronic systems with higher safety, higher biocompatibility, and smaller size have received extensive attentions. Nanogenerator has received widespread attention because it can collect and store various energies in the environment, and can provide long-term, low-maintenance, and self-powered energy for micro-nano systems.[5,6] Common nanogenerator comprising triboelectric nanogenerator (TENG),[7−19] piezoelectric nanogenerator,[20−30] and pyroelectric nanogenerator.[31−35] Among them, TENG has a unique advantage because of its high output voltage, applicable working frequency, and high efficiency. It can reach an open circuit voltage of several thousand volts and can be used to induce gas discharge to generate plasma,[36−40] but there is a certain risk of electrostatic discharge (ESD) in a nonoperating environment. To prevent ESD, the nonoperating voltage of TENG should be less than 30 V.[41]

Electrospinning technology is simple and portable, and its ability to prepare nanofibers is stable and fast,[42] so it can be used to prepare TENG to meet various application needs. On the basis of this technology, the structure of the fiber can be adjusted by adding auxiliary electrodes and improving the collection device. For example, the preparation of single fibers can be prepared by using near-field electrospinning technology,[43,44] while ordered nanofibers can be collected by parallel electrodes or high-speed drum.[45,46] From the point of view of physical theory, as the order of the fiber structure increases, its mechanical strength will improve.[47]

In this study, we use high-speed drum to obtain ordered nanofibers as the friction layer of TENG, which significantly improves the tensile properties and mechanical strength of the TENG, at the same time, the nanogenerator has anisotropic properties. Adjusting the friction angle to change the contact area of the anisotropic triboelectric nanogenerator (A-TENG) during friction, after the two friction layers rotate 90 degrees, the output voltage of the A-TENG will change by an order of magnitude. Therefore, when the nanogenerator is not used, it can be rotated to avoid electrostatic discharge. It has good prospect in the wearable field.

2. EXPERIMENTAL SECTION

2.1. Materials. Nylon 6 (PA6) powders were provided by Macklin Biochemical Co., Ltd. (China) and polyvinylidene fluoride (PVDF) powders (Mw ∼1,000,000) used in this study were provided by Shanghai 3F New Materials Co., Ltd.. *N*,*N*-Dimethylformamide

Received: August 3, 2020
Accepted: September 16, 2020
Published: September 16, 2020

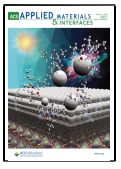

https://dx.doi.org/10.1021/acsami.0c13938
ACS Appl. Mater. Interfaces 2020, 12, 46205−46211

(DMF), ethanol, acetic acid, and formic acid were provided by Sinopharm Chemical Reagents. Acetone was provided by Laiyang Fine Chemical Plant.

2.2. Preparation of Solutions for Electrospinning. Dissolve PVDF powder in a mixed solvent of DMF-acetone (1:1 by weight) and stir continuously at 45 °C for 4 h to prepare a homogeneous PVDF solution (10 wt %). Dissolve PA6 powder in a mixed solvent of acetic acid-formic acid solvent (1:1 by weight) and stir continuously for 5 h to obtain a transparent PA6 solution (15 wt %).

2.3. Fabrication of the NG. Figure 1a shows the electrospinning device. PA6 nanofiber membrane and PVDF nanofiber membrane

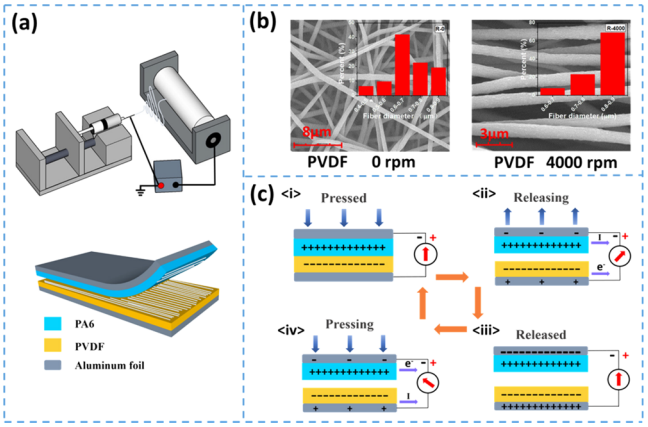

Figure 1. (a) Electrospinning device diagram and structure diagram of A-TENG. (b) SEM characterization and statistical distribution of fiber diameter of PVDF nanofibers at 0 and 4000 rpm. (c) Generator mechanism of contact separation type TENG.

were prepared as the friction layer of TENG by electrospinning technology. The PVDF fiber membrane was obtained under the preparation environment of 45 ± 5% humidity and 24 ± 2 °C temperature. The needle used has an inner diameter of 0.6 mm and an outer diameter of 0.91 mm. The electrospinning solution was 5 mL. The polymer solution was discharged at a constant flow rate of 1 mL h^{-1}, a high voltage of 15 kV was applied to the syringe needle, the spinning distance was 15 cm, and the rotating speed of the drum was adjusted to collect nanofibers in an orderly arrangement. The PA6 fiber membrane was obtained under the preparation environment of 43 ± 5% humidity and 24 ± 3 °C temperature, the liquid supply rate was 0.5 mL h^{-1}, applied a voltage of 20 kV, the spinning distance was 18 cm, and collected nanofibers through aluminum foil and drum.

2.4. Characterization and Measurements. The microstructure and morphology of TENG were characterized by the scanning electron microscope (SEM, JEOL, JSM-6700F), and the diameter of the electrospun nanofiber membrane was measured with Nano Measurer software. The TENG was tested for stress and strain by Instron 3300 Universal Testing Systems. The crystal structure of PA6 and PVDF was characterized by Fourier transform infrared spectroscopy (FTIR, Thermo Scientific Nicolet iN10). The output voltage signal of TENG was recorded through a digital oscilloscope (GDS-2102, Gwinstek). The output current signal was recorded by a digital oscilloscope (GDS-2102, Gwinstek) and a current amplifier (SR570). The charging voltage of commercial capacitors was recorded with a digital multimeter (Rigol DM 3058). To measure the triboelectricity generated by NG, a periodic friction device was built, Supporting Information, Figure S1 shows a model diagram of the device.

3. RESULTS AND DISCUSSION

3.1. The Basic Characterization of the TENG. Electrospinning is carried out through the device as shown in Figure 1a to obtain nanofiber membranes. The electrospinning equipment is mainly composed of a propulsion pump, a power supply, and a drum collector. Two friction layers and two electrodes form a simple TENG. A layer of metal aluminum foil is fixed on the drum collector as the electrode material of the nanogenerator. Due to the difference in electron affinity, PA6 nanofiber membrane is selected as the positive friction layer of TENG, PVDF nanofiber membrane as a negative friction layer. The higher the speed of the drum collector, the more ordered the nanofibers obtained. When the drum is not used (R-0) and the drum speed is 4000 rpm (R-4000), the fiber morphology of PVDF nanofibers obtained by electrospinning is shown in Figure 1b. When R-0, the nanofibers present a disordered state, and the average fiber diameter is 690 nm, while when R-4000, the average fiber diameter is 830 nm, and the fibers present an orderly arrangement state. Supporting Information, Figure S2 shows the (a) SEM image and (b) fiber diameter distribution of PA6 fibers. The drum speed is 4000 rpm with an average diameter of 840 nm.

TENG realizes the conversion of mechanical energy to electrical energy based on the coupling of triboelectric effect and electrostatic induction effect. As shown in Figure 1c, in the starting state (state i), the two friction planes touch each other. Due to the difference in electron affinity, the electrons on the surface of the PA6 friction layer are transferred to the PVDF friction layer, thereby leaving a static negative charge on the surface of the negative friction layer and a static positive charge on the surface of the positive friction layer, achieving electrostatic balance, at which time there is no current and potential difference. With the separation of the positive and negative friction layers, the relative movement between the opposite charges occurs, and a potential difference is generated between the two electrodes. To re-realize the electrostatic equilibrium state, the free electrons between the electrodes flow, resulting in a current flow (state ii). When the separation distance of the two friction layers reaches the maximum, the current goes down to 0 (state iii). When pressure is applied again, the amount of induced charge on the electrode decreases as the separation distance decreases, and the current reverses (state iv).[36,48]

The longitudinal direction is along the direction of the rotating of the drum, and the lateral direction is perpendicular to the direction of the rotating of the drum. As shown in Figure 2, the PVDF ordered fibers (R-4000) and random fibers (R-0),

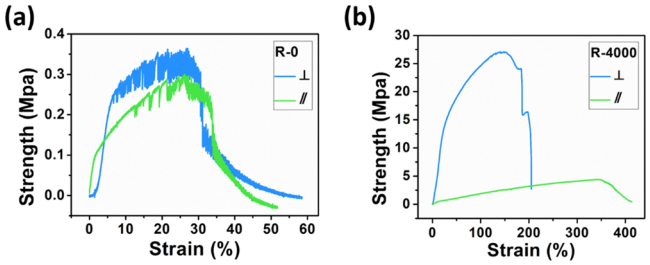

Figure 2. Tensile properties of PVDF nanofibers at (a) 0 rpm and (b) 4000 rpm.

obtained by electrospinning technology, were tested for the tensile properties of the film in the transverse and longitudinal directions, respectively. The environmental humidity was 55 ± 2%, the temperature was 24 ± 2 °C, the stretching rate was 2 mm min^{-1}, and the test sample size was 2 cm × 1 cm. By the formula

$$P = F/hd \quad (1)$$

https://dx.doi.org/10.1021/acsami.0c13938
ACS Appl. Mater. Interfaces 2020, 12, 46205−46211

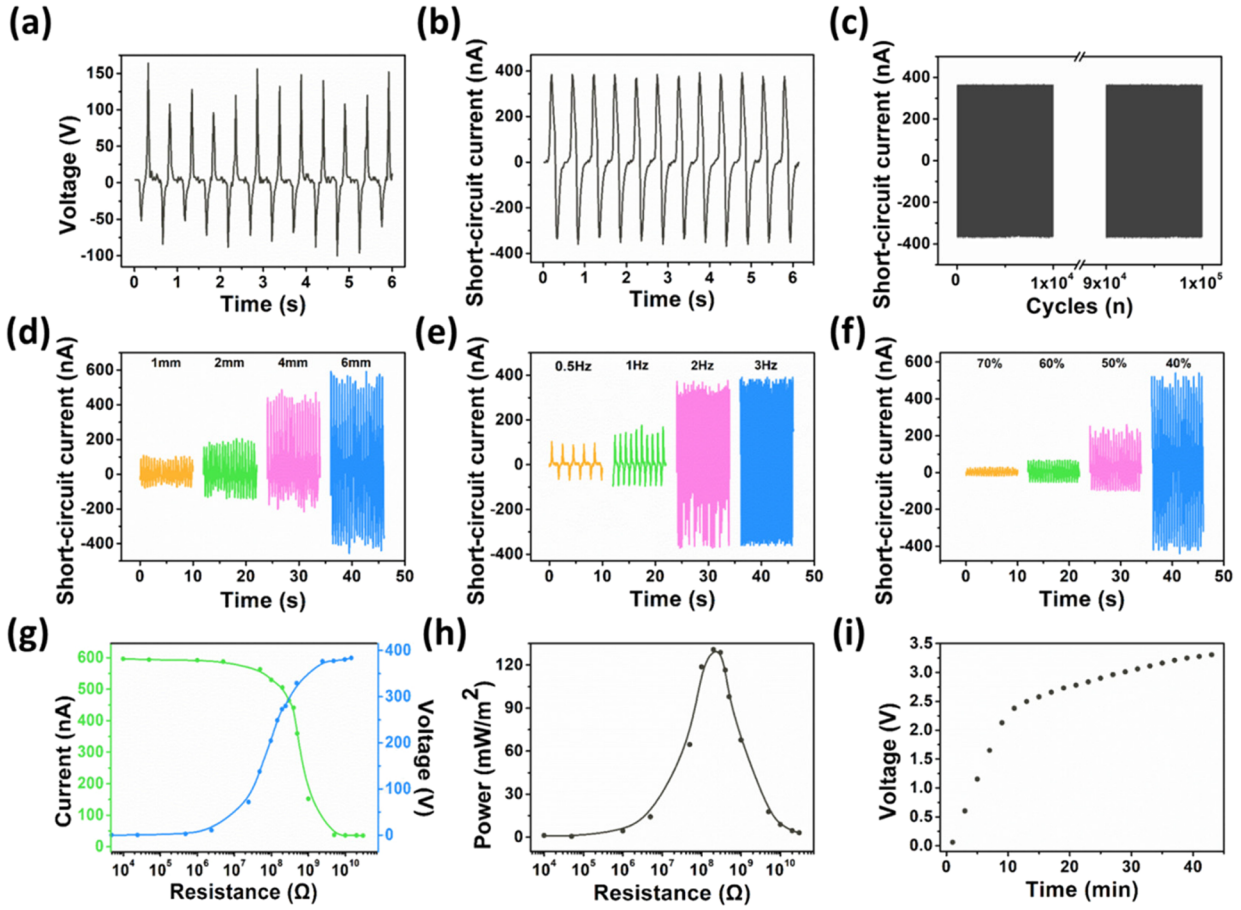

Figure 3. Electrical performance of TENG. (a) Open circuit voltage. (b) Short-circuit current. (c) Durability and stability test of TENG. The short-circuit current under changes in (d) separation distance between friction layers, (e) impact frequency, and (f) ambient humidity. (g) Output voltage and current of TENG under external load resistance. (h) Relationship between load resistance and output power. (i) Commercial capacitor (47 μF) is charged by TENG.

to get the tensile properties, where h and d represent the thickness and width of the tested PVDF fiber membrane, respectively. The thickness of the sample is shown in the Supporting Information, Figure S3. PVDF nanofibers are arranged in disorder at R-0, and two mutually perpendicular directions are randomly selected as transverse and longitudinal directions, the tensile properties between the transverse and longitudinal directions are not different; the longitudinal tensile strength is about 0.36 Mpa. For R-4000, the longitudinal tensile strength is significantly improved and can reach 27 Mpa, while the transverse tensile strength is relatively small, only 4.38 Mpa, as shown in Figure 2b, which shows obvious anisotropy.

High-speed drum is used to obtain ordered nanofibers, the order degree of fiber arrangement increases, and the tensile strength along the longitudinal direction is greatly enhanced. This is because under tensile load, with the increase of porosity and disorder, the state of the single pore stress concentration control gradually transits to the state of porous interaction.[45] The structure of the material was analyzed by FTIR test, as shown in the Supporting Information, Figure S4a,b.

3.2. The Electrical Performance of TENG. We systematically measured the electrical signals of device with an area of 16 cm^2 (40 mm × 40 mm) to evaluate the performance of anisotropic TENG (A-TENG) for motion detection and environmental mechanical energy collection. The thickness of the PVDF and PA6 friction layers are 0.026 and 0.018 mm, respectively. To ensure the scientificity of the experiment, we tested the same pair of samples throughout the experiment. As shown in the Supporting Information, Figure S1, A-TENG adopted a non-grounded measurement configuration,[49] through a self-made periodic friction device to achieve continuous contact separation, Figure 3 shows the test results. Figure 3a,b shows the measured open-circuit voltage and short-circuit current under an environment with an impact frequency of 2 Hz, a humidity of 45%, and a friction separation distance of 4 mm, which can reach 164 V and 392 nA, respectively.

The stability and durability of the equipment are necessary factors for TENG in practical applications. A-TENG has been tested for 100,000 cycles under an environment with an impact frequency of 2 Hz, a humidity of 47%, and a friction separation distance of 4 mm. As shown in Figure 3c, the short-circuit current did not change significantly before and after the cycle test, indicating that A-TENG has good stability.

Considering the influence of the working environment on the device, the environmental adaptability of the manufactured A-TENG was evaluated, tested the performance of A-TENG under different separation distances between friction layers, impact frequencies, and ambient humidity. In the whole test process, a comparative experiment was conducted using the control variable method. As shown in Figure 3d, the short-circuit current decreases as the friction separation distance decreases.[50] As shown in Figure 3e, as the friction frequency increases, the short-circuit current increases. This is because

https://dx.doi.org/10.1021/acsami.0c13938
ACS Appl. Mater. Interfaces 2020, 12, 46205−46211

the increase in the impact frequency shortens the duration of the peak value, while the total charge transferred by the external circuit is constant, thereby increasing the short-circuit current. Similarly, the open-circuit voltage increases with increasing separation distance and impact frequency, as shown in the Supporting Information, Figure S5a,b. As shown in Figure 3f and in the Supporting Information, Figure S5c, a higher humidity environment will reduce the residence time of the charge on the friction surface, thus reducing the output.[51]

To be better used in practical applications, we have studied the current and voltage signals of A-TENG under different load resistances. The voltage gradually increases as the load resistance increases, and the current decreases as the load resistance increases, as shown in Figure 3g. As shown in Figure 3h, we fitted the instantaneous power density curve through the equation $P = \frac{U^2}{R}$. When the external load resistance is 226.4 MΩ, the maximum load power density is obtained, which is 129.46 mW m^{-2}.

As shown in Figure 3i, the pulse energy of A-TENG can be collected and stored; A-TENG can charge a commercial capacitor of 47 μF to 3.3 V under the conditions of an environmental humidity of 45%, a friction layer separation distance of 6 mm, and an impact frequency of 3 Hz. It can meet the electricity demand of small portable intelligent electronic devices.

As a device that can efficiently collect various forms of energy, A-TENG can supply power to many common electronic devices. A-TENG with an area of 4 cm × 4 cm was selected for a visual demonstration. A-TENG can charge a 47 μF commercial capacitor to 3 V to meet the electricity demand of small smart electronic devices, such as electronic watches and temperature-humidity sensors, as shown in Figure 4a,b, the demonstration experiment are shown in the Supporting Information, Video S1 and S2. As shown in Figure 4c, A-TENG can light up wave-shaped LEDs, the demonstration experiment is shown in the Supporting Information, Video S3. The test results show that A-TENG has good development potential in terms of energy harvesting.

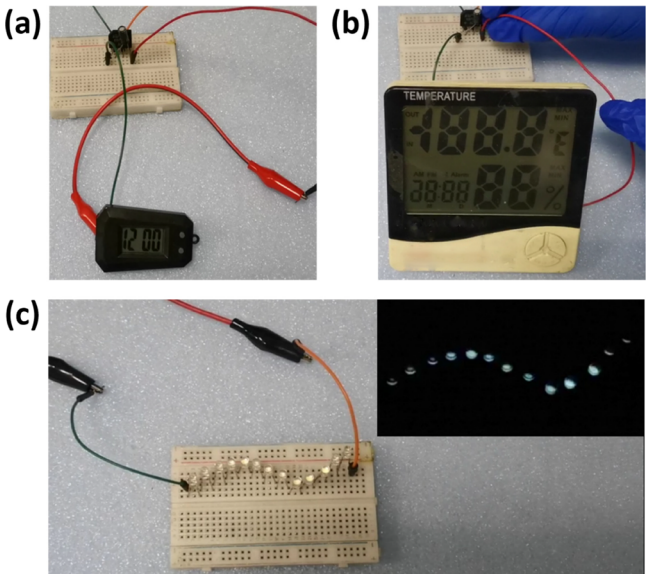

Figure 4. Application of A-TENG in small electronic equipment. A-TENG can drive (a) electronic watches and (b) temperature–humidity sensors. (c) Light up the wave-shaped LED.

3.3. The Application of A-TENG. There are serious safety hazards in ESD in production and life. When the static object with high voltage is in contact with other objects, there is a charge flow according to the mechanism of charge neutralization, which transfers enough power to offset the voltage. During the transmission of power in this high speed process, potential voltages, currents, and electromagnetic fields are generated. In severe cases, objects are destroyed, which causes ESD damage. This safety hazard also exists in A-TENG, which has high-voltage output capabilities. Air is ionized and converted into plasma under the action of high voltage, showing the characteristics of electrical conductivity. The charges on the two contact surfaces are conducted to each other through the ionized air channel, resulting in ESD. When the electrostatic discharge phenomenon is detected by the auxiliary light detecting module, the ESD phenomenon of TENG is easily observed.[52] As shown in Figure 5a, under nonoperating environment, due to the large difference in electronegativity between the two friction layers of TENG, unexpected friction may occur. The high voltage generated by the accumulation of charge on the surface will bring electrostatic discharge to the nearby circuits (ESD) risk. To prevent this unsafe event from happening, an embedded A-TENG was designed, as shown in Figure 5b. For A-TENG, changing the friction direction of the nanofiber membrane, the effective contact area changes, and the size of the output signal will changes accordingly. By reducing the charge of electrostatic objects, ESD hazards can be effectively avoided. The reducing of charge on nanogenerator can be reflected by the drop of its output. Supporting Information, Video S4 demonstrates the state of the small bulb in different working modes of A-TENG, when the voltage is too high, the small bulb is burnt.

When embedded, the A-TENG can work normally to supply current to the circuit. The output voltage is approximately 216.13 V, as shown in Figure 5c, and the output current is about 510 nA, as shown in the Supporting Information, Figure S6a, making it a good power source.

When placed vertically (or not embedded), as shown in Figure 5d the friction produces a voltage of approximately 28 V, which is much smaller than the output voltage when embedded. Similarly, as shown in the Supporting Information, Figure S6b, the output current is about 23 nA, which is much smaller than the output current when embedded, this is not enough to penetrate the gas. So when not in use, A-TENG can be rotated vertically to set the insurance. In this case, A-TENG can no longer output high voltage even if the mechanical contact continues. Locked A-TENG can greatly reduce the risk of ESD in case of accidental contact in an open-circuit situation. When the nanogenerator is restored, the two electrodes can be returned to their original angle and the nanogenerator can continue to output. Since nanogenerator is widely used in wearable systems, electrode contact in a flexible environment is unavoidable, and this design can prevent idle nanogenerator from continuing to accumulate charge and burn the power supply circuit.

It can be seen that A-TENG is more secure than ordinary TENG, and the output anisotropy plays a role in insurance. Without adding additional devices, it greatly reduces the hidden safety hazards of surrounding instruments and better prevents them. To prevent the occurrence of danger, while

https://dx.doi.org/10.1021/acsami.0c13938
ACS Appl. Mater. Interfaces 2020, 12, 46205−46211

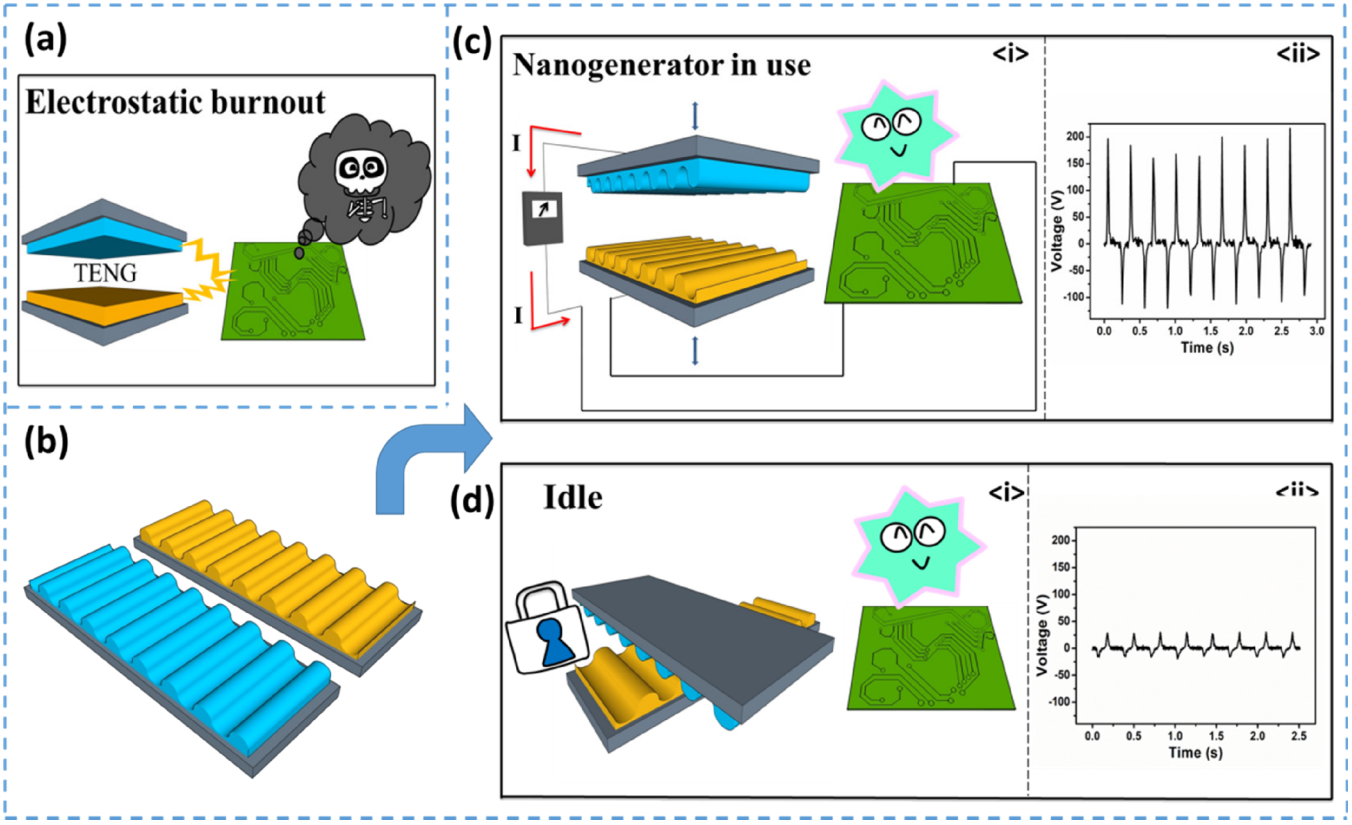

Figure 5. (a) Accumulation of charge causes the circuit to burn out. (b) Embedded electrode model. (c) For the embedded A-TENG, the accumulated charge can be used to power the circuit. (d) If the A-TENG is not needed, it can be locked by rotating 90° and the output will drop to a safe level in case the two layers contact by accident.

maintaining the high output of TENG under normal conditions, and the operation is simple and feasible, therefore, the emergence of this new type of TENG has made nanogenerator a mature and reliable energy source with great potential for development in wearable and flexible electronic devices.

4. CONCLUSIONS

In short, we used electrospinning technology, combined with high-speed drum, collected oriented polymer nanofibers, and obtained A-TENG. Under the stress dispersion effect of ordered fiber, the tensile properties and strength of A-TENG have been significantly improved, and also has obvious anisotropy. The open-circuit voltage and short-circuit current of A-TENG can reach 164 V and 392 nA, and the maximum output power density can reach 129.46 mW m^{-2}. A-TENG can directly light the LED, by charging the 47 μF capacitor; the nanogenerator powers the electronic watch and the temperature and humidity sensor. Changing the relative direction of friction of the nanofiber membrane will change the size of the output signal. The A-TENG can be rotated and locked to prevent circuit burnout.

■ ASSOCIATED CONTENT

Supporting Information

The Supporting Information is available free of charge at https://pubs.acs.org/doi/10.1021/acsami.0c13938.

Schematic diagram of the TENG test set, SEM image and diameter distribution of PA6 nanofibers, thickness of the sample subjected to the tensile test, the FTIR of PVDF fiber membranes and PA6 fiber membranes, the open circuit voltage of TENG under different conditions, and current output of the embedded A-TENG (PDF)

Video demonstrating the experiment of A-TENG drive electronic watches (MP4)

Video demonstrating experiment of A-TENG drive temperature-humidity sensors (MP4)

Video demonstrating the experiment of A-TENG light up LEDs (MP4)

Video demonstrating the state of the small bulbs of A-TENG in different working modes (MP4)

■ AUTHOR INFORMATION

Corresponding Author

Yun-Ze Long − *Collaborative Innovation Center for Nanomaterials & Devices, College of Physics and Collaborative Innovation Center for Eco-Textiles of Shandong Province, Qingdao University, Qingdao 266071, China;* orcid.org/0000-0002-4278-4515; Email: yunze.long@qdu.edu.cn, yunze.long@163.com

Authors

Ning Wang − *Collaborative Innovation Center for Nanomaterials & Devices, College of Physics, Qingdao University, Qingdao 266071, China*

Xiao-Xiong Wang − *Collaborative Innovation Center for Nanomaterials & Devices, College of Physics, Qingdao University, Qingdao 266071, China*

https://dx.doi.org/10.1021/acsami.0c13938
ACS Appl. Mater. Interfaces 2020, 12, 46205−46211

Kang Yan − *Collaborative Innovation Center for Nanomaterials & Devices, College of Physics, Qingdao University, Qingdao 266071, China*
Weizhi Song − *Collaborative Innovation Center for Nanomaterials & Devices, College of Physics, Qingdao University, Qingdao 266071, China*
Zhiyong Fan − *Department of Electronic & Computer Engineering, The Hong Kong University of Science & Technology, Kowloon, Hong Kong, China;* orcid.org/0000-0002-5397-0129
Miao Yu − *Collaborative Innovation Center for Nanomaterials & Devices, College of Physics, Qingdao University, Qingdao 266071, China; Junada (Qingdao) Technology Co., Ltd, Qingdao International Academician Park, Qingdao 266199, China*

Complete contact information is available at: https://pubs.acs.org/10.1021/acsami.0c13938

Author Contributions

[⊥]N.W. and X.-X.W. contributed equally to this work.

Notes

The authors declare no competing financial interest.

■ ACKNOWLEDGMENTS

This work was supported by the National Natural Science Foundation of China (51673103, 51973100, and 11847135), the National Key Research Development Project (2019YFC0121402), and State Key Laboratory of Bio-Fibers and Eco-Textiles (Qingdao University, ZKT46).

■ REFERENCES

(1) Wu, C.; Wang, A. C.; Ding, W.; Guo, H.; Wang, Z. L. Triboelectric Nanogenerator: A Foundation of the Energy for the New Era. *Adv. Energy Mater.* **2019**, *9*, 1802906.
(2) Jiang, D.; Shi, B.; Ouyang, H.; Fan, Y.; Wang, Z.; Li, Z. Emerging Implantable Energy Harvesters and Self-Powered Implantable Medical Electronics. *ACS Nano* **2020**, *14*, 6436−6448.
(3) Cao, M.; Fan, S.; Qiu, H.; Su, D.; Li, L.; Su, J. CB Nanoparticles Optimized 3D Wearable Graphene Multifunctional Piezoresistive Sensor Framed by Loofah Sponge. *ACS Appl. Mater. Interfaces* **2020**, *12*, 36540−36547.
(4) Cao, M.; Su, J.; Fan, S.; Qiu, H.; Su, D.; Li, L. Wearable Piezoresistive Pressure Sensors Based on 3D Graphene. *Chem. Eng. J.* **2020**, *406*, 126777.
(5) Jiang, D.; Shi, B.; Ouyang, H.; Fan, Y.; Wang, Z. L.; Chen, Z.-M.; Li, Z. A 25-year Bibliometric Study of Implantable Energy Harvesters and Self-Powered Implantable Medical Electronics Researches. *Mater. Today Energy* **2020**, *16*, 100386.
(6) Sun, J.; Yang, A.; Zhao, C.; Liu, F.; Li, Z. Recent Progress of Nanogenerators Acting as Biomedical Sensors in Vivo. *Sci. Bull.* **2019**, *64*, 1336−1347.
(7) Bai, Y.; Xu, L.; Lin, S.; Luo, J.; Qin, H.; Han, K.; Wang, Z. L. Charge Pumping Strategy for Rotation and Sliding Type Triboelectric Nanogenerators. *Adv. Energy Mater.* **2020**, *10*, 2000605.
(8) Chen, H.; Koh, J. J.; Liu, M.; Li, P.; Fan, X.; Liu, S.; Yeo, J. C. C.; Tan, Y.; Tee, B. C. K.; He, C. Super Tough and Self-Healable Poly(dimethylsiloxane) Elastomer via Hydrogen Bonding Association and Its Applications as Triboelectric Nanogenerators. *ACS Appl. Mater. Interfaces* **2020**, *12*, 31975−31983.
(9) Han, C.; Zhang, C.; Tang, W.; Li, X.; Wang, Z. L. High Power Triboelectric Nanogenerator Based on Printed Circuit Board (PCB) Technology. *Nano Res.* **2015**, *8*, 722−730.
(10) Huang, L.-B.; Xu, W.; Zhao, C.; Zhang, Y.-L.; Yung, K.-L.; Diao, D.; Fung, K. H.; Hao, J. Multifunctional Water Drop Energy Harvesting and Human Motion Sensor Based on Flexible Dual-Mode Nanogenerator Incorporated with Polymer Nanotubes. *ACS Appl. Mater. Interfaces* **2020**, *12*, 24030−24038.
(11) Liu, W.; Wang, Z.; Wang, G.; Liu, G.; Chen, J.; Pu, X.; Xi, Y.; Wang, X.; Guo, H.; Hu, C.; Wang, Z. L. Integrated Charge Excitation Triboelectric Nanogenerator. *Nat. Commun.* **2019**, *10*, 11426.
(12) Long, Y.; Chen, Y.; Liu, Y.; Chen, G.; Guo, W.; Kang, X.; Pu, X.; Hu, W.; Wang, Z. L. A Flexible Triboelectric Nanogenerator Based on a Super-Stretchable and Self-Healable Hydrogel as the Electrode. *Nanoscale* **2020**, *12*, 12753−12759.
(13) Wang, Z. L. On Maxwell's Displacement Current for Energy and Sensors: the Origin of Nanogenerators. *Mater. Today* **2017**, *20*, 74−82.
(14) Wang, Z. L.; Chen, J.; Lin, L. Progress in Triboelectric Nanogenerators as a New Energy Technology and Self-Powered Sensors. *Energy Environ. Sci.* **2015**, *8*, 2250−2282.
(15) Meng, J.; Li, H.; Zhao, L.; Lu, J.; Pan, C.; Zhang, Y.; Li, Z. Triboelectric Nanogenerator Enhanced Schottky Nanowire Sensor for Highly Sensitive Ethanol Detection. *Nano Lett.* **2020**, *20*, 4968−4974.
(16) Bu, C.; Li, F.; Yin, K.; Pang, J.; Wang, L.; Wang, K. Research Progress and Prospect of Triboelectric Nanogenerators as Self-Powered Human Body Sensors. *ACS Appl. Electron. Mater.* **2020**, *2*, 863−878.
(17) Shi, B.; Liu, Z.; Zheng, Q.; Meng, J.; Ouyang, H.; Zou, Y.; Jiang, D.; Qu, X.; Yu, M.; Zhao, L.; Fan, Y.; Wang, Z. L.; Li, Z. Body-Integrated Self-Powered System for Wearable and Implantable Applications. *ACS Nano* **2019**, *13*, 6017−6024.
(18) Ouyang, H.; Tian, J.; Sun, G.; Zou, Y.; Liu, Z.; Li, H.; Zhao, L.; Shi, B.; Fan, Y.; Fan, Y.; Wang, Z. L.; Li, Z. Self-Powered Pulse Sensor for Antidiastole of Cardiovascular Disease. *Adv. Mater.* **2017**, *29*, 1703456.
(19) Zhao, L.; Li, H.; Meng, J.; Wang, A. C.; Tan, P.; Zou, Y.; Yuan, Z.; Lu, J.; Pan, C.; Fan, Y.; Zhang, Y.; Zhang, Y.; Wang, Z. L.; Li, Z. Reversible Conversion between Schottky and Ohmic Contacts for Highly Sensitive, Multifunctional Biosensors. *Adv. Funct. Mater.* **2020**, *30*, 1907999.
(20) Chung, S. Y.; Kim, S.; Lee, J. H.; Kim, K.; Kim, S. W.; Kang, C. Y.; Yoon, S. J.; Kim, Y. S. All-Solution-Processed Flexible Thin Film Piezoelectric Nanogenerator. *Adv. Mater.* **2012**, *24*, 6022−6027.
(21) Hu, D.; Yao, M.; Fan, Y.; Ma, C.; Fan, M.; Liu, M. Strategies to Achieve High Performance Piezoelectric Nanogenerators. *Nano Energy* **2019**, *55*, 288−304.
(22) Huan, Y.; Zhang, X.; Song, J.; Zhao, Y.; Wei, T.; Zhang, G.; Wang, X. High-Performance Piezoelectric Composite Nanogenerator Based on Ag/(K, Na)NbO3 Heterostructure. *Nano Energy* **2018**, *50*, 62−69.
(23) Karan, S. K.; Bera, R.; Paria, S.; Das, A. K.; Maiti, S.; Maitra, A.; Khatua, B. B. An Approach to Design Highly Durable Piezoelectric Nanogenerator Based on Self-Poled PVDF/AlO-rGO Flexible Nanocomposite with High Power Density and Energy Conversion Efficiency. *Adv. Energy Mater.* **2016**, *6*, 201601016.
(24) Pi, Z.; Zhang, J.; Wen, C.; Zhang, Z.-B.; Wu, D. Flexible Piezoelectric Nanogenerator Made of Poly(vinylidenefluoride-co-trifluoroethylene) (PVDF-TrFE) Thin Film. *Nano Energy* **2014**, *7*, 33−41.
(25) Ren, X.; Fan, H.; Zhao, Y.; Liu, Z. Flexible Lead-Free BiFeO3/PDMS-Based Nanogenerator as Piezoelectric Energy Harvester. *ACS Appl. Mater. Interfaces* **2016**, *8*, 26190−26197.
(26) Wang, X.; Song, J.; Liu, J.; Wang, Z. L. Direct-Current Nanogenerator Driven by Ultrasonic Waves. *Science* **2007**, *316*, 102−105.
(27) Wang, X.; Song, W.-Z.; You, M.-H.; Zhang, J.; Yu, M.; Fan, Z.; Ramakrishna, S.; Long, Y. Z. Bionic Single-Electrode Electronic Skin Unit Based on Piezoelectric Nanogenerator. *ACS Nano* **2018**, *12*, 8588−8596.
(28) Zhang, L.; Bai, S.; Su, C.; Zheng, Y.; Qin, Y.; Xu, C.; Wang, Z. L. A High-Reliability Kevlar Fiber-ZnO Nanowires Hybrid Nanogenerator and its Application on Self-Powered UV Detection. *Adv. Funct. Mater.* **2015**, *25*, 5794−5798.

(29) Liu, Q.; Wang, X. X.; Song, W. Z.; Qiu, H. J.; Zhang, J.; Fan, Z.; Yu, M.; Long, Y. Z. Wireless Single-Electrode Self-Powered Piezoelectric Sensor for Monitoring. *ACS Appl. Mater. Interfaces* **2020**, *12*, 8288−8295.
(30) Liu, Z.; Xu, L.; Zheng, Q.; Kang, Y.; Shi, B.; Jiang, D.; Li, H.; Qu, X.; Fan, Y.; Wang, Z. L.; Li, Z. Human Motion Driven Self-Powered Photodynamic System for Long-Term Autonomous Cancer Therapy. *ACS Nano* **2020**, *14*, 8074−8083.
(31) Gao, F.; Li, W.; Wang, X.; Fang, X.; Ma, M. A Self-Sustaining Pyroelectric Nanogenerator Driven by Water Vapor. *Nano Energy* **2016**, *22*, 19−26.
(32) Qi, J.; Ma, N.; Yang, Y. Photovoltaic-Pyroelectric Coupled Effect Based Nanogenerators for Self-Powered Photodetector System. *Adv. Mater. Interfaces* **2018**, *5*, 201701189.
(33) Wang, X.; Dai, Y.; Liu, R.; He, X.; Li, S.; Wang, Z. L. Light-Triggered Pyroelectric Nanogenerator Based on a pn-Junction for Self-Powered Near Infrared Photosensing. *ACS Nano* **2017**, *11*, 8339−8345.
(34) Yang, Y.; Zhou, Y.; Wu, J. M.; Wang, Z. L. Single Micro/Nanowire Pyroelectric Nanogenerators as Self-Powered Temperature Sensors. *ACS Nano* **2012**, *6*, 8456−8461.
(35) You, M. H.; Wang, X. X.; Yan, X.; Zhang, J.; Song, W. Z.; Yu, M.; Fan, Z. Y.; Ramakrishna, S.; Long, Y. Z. A Self-Powered Flexible Hybrid Piezoelectric-Pyroelectric Nanogenerator Based on Non-Woven Nanofiber Membranes. *J. Mater. Chem. A* **2018**, *6*, 3500−3509.
(36) Qiu, H.-J.; Song, W.-Z.; Wang, X.-X.; Zhang, J.; Fan, Z.; Yu, M.; Ramakrishna, S.; Long, Y. Z. A Calibration-Free Self-Powered Sensor for Vital Sign Monitoring and Finger Tap Communication Based on Wearable Triboelectric Nanogenerator. *Nano Energy* **2019**, *58*, 536−542.
(37) Yang, F.; Guo, J.; Zhao, L.; Shang, W.; Gao, Y.; Zhang, S.; Gu, G.; Zhang, B.; Cui, P.; Cheng, G.; Du, Z. Tuning Oxygen Vacancies and Improving UV Sensing of ZnO Nanowire by Micro-Plasma Powered by a Triboelectric Nanogenerator. *Nano Energy* **2020**, *67*, 104210.
(38) Yang, F.; Zheng, M.; Zhao, L.; Guo, J.; Zhang, B.; Gu, G.; Cheng, G.; Du, Z. The High-Speed Ultraviolet Photodetector of ZnO Nanowire Schottky Barrier Based on the Triboelectric-Nanogenerator-Powered Surface-Ionic-Gate. *Nano Energy* **2019**, *60*, 680−688.
(39) Zhao, L.; Chen, K.; Yang, F.; Zheng, M.; Guo, J.; Gu, G.; Zhang, B.; Qin, H.; Cheng, G.; Du, Z. The Novel Transistor and Photodetector of Monolayer MoS2 Based on Surface-Ionic-Gate Modulation Powered by a Triboelectric Nanogenerator. *Nano Energy* **2019**, *62*, 38−45.
(40) Zheng, M.; Yang, F.; Guo, J.; Zhao, L.; Jiang, X.; Gu, G.; Zhang, B.; Cui, P.; Cheng, G.; Du, Z. $Cd(OH)_2$@ZnO Nanowires Thin-Film Transistor and UV Photodetector with a Floating Ionic Gate Tuned by a Triboelectric Nanogenerator. *Nano Energy* **2020**, *73*, 104808.
(41) *Electrostatic discharge* https://encyclopedia.thefreedictionary.com/Electrostatic+discharge
(42) Dong, W. H.; Liu, J. X.; Mou, X. J.; Liu, G. S.; Huang, X. W.; Yan, X.; Ning, X.; Russell, S. J.; Long, Y. Z. Performance of Polyvinyl Pyrrolidone-Isatis Root Antibacterial Wound Dressings Produced in Situ by Handheld Electrospinner. *Colloid Surf. B-Biointerfaces* **2020**, *188*, 110766.
(43) Bisht, G. S.; Canton, G.; Mirsepassi, A.; Kuinsky, L.; Oh, S.; Dunn-Rankin, D.; Madou, M. J. Controlled Continuous Patterning of Polymeric Nanofibers on Three-Dimensional Substrates Using Low-Voltage Near-Field Electrospinning. *Nano Lett.* **2011**, *11*, 1831−1837.
(44) Sun, D.; Chang, C.; Li, S.; Lin, L. Near-field Electrospinning. *Nano Lett.* **2006**, *6*, 839−842.
(45) Katta, P.; Alessandro, M.; Ramsier, R. D.; Chase, G. G. Continuous Electrospinning of Aligned Polymer Nanofibers onto a Wire Drum Collector. *Nano Lett.* **2004**, *4*, 2215−2218.
(46) Li, D.; Wang, Y.; Xia, Y. Electrospinning of Polymeric and Ceramic Nanofibers as Uniaxially Aligned Arrays. *Nano Lett.* **2003**, *3*, 1167−1171.
(47) Laubie, H.; Radjai, F.; Pellenq, R.; Ulm, F. J. Stress Transmission and Failure in Disordered Porous Media. *Phys. Rev. Lett.* **2017**, *119*, No. 075501.
(48) Li, Z.; Shen, J.; Abdalla, I.; Yu, J.; Ding, B. Nanofibrous Membrane Constructed Wearable Triboelectric Nanogenerator for High Performance Biomechanical Energy Harvesting. *Nano Energy* **2017**, *36*, 341−348.
(49) Zhang; Gu, G.; Qin, H.; Li, S.; Shang, W.; Wang, T.; Zhang, B.; Cui, P.; Guo, J.; Yang, F.; Cheng, G.; Du, Z. Measuring the Actual Voltage of a Triboelectric Nanogenerator Using the Non-Grounded Method. *Nano Energy* **2020**, *77*, 105108.
(50) Niu, S.; Wang, Z. L. Theoretical Systems of Triboelectric Nanogenerators. *Nano Energy* **2015**, *14*, 161−192.
(51) Nguyen, V.; Zhu, R.; Yang, R. Environmental Effects on Nanogenerators. *Nano Energy* **2015**, *14*, 49−61.
(52) Su, Z.; Han, M.; Cheng, X.; Chen, H.; Chen, X.; Zhang, H. Asymmetrical Triboelectric Nanogenerator with Controllable Direct Electrostatic Discharge. *Adv. Funct. Mater.* **2016**, *26*, 5524−5533.

https://dx.doi.org/10.1021/acsami.0c13938
ACS Appl. Mater. Interfaces 2020, 12, 46205−46211